Lattice dynamics calculations and phonon dispersion measurements of zircon, $ZrSiO_4$

R. Mittal and S. L. Chaplot
Solid State Physics Division, Bhabha Atomic Research Centre, Trombay, Mumbai 400 085, India

R. Parthasarathy
Analytical Chemistry Division, Bhabha Atomic Research Centre, Trombay, Mumbai 400 085, India

M. J. Bull
Rutherford Appleton Laboratory, Chilton, Didcot, OX11 0QX, United Kingdom

M. J. Harris
Ripon College Cuddesdon, Oxford, OX44 9EX, United Kingdom
(Received 3 February 2000; revised manuscript received 25 July 2000)

Lattice dynamical calculations using a shell model are carried out for the geophysically important mineral zircon, $ZrSiO_4$. The model parameters are adjusted so that the model satisfactorily reproduces the literature data on structure, elastic constants and optically active modes. Phonon dispersion relations are measured on a single crystal using coherent-inelastic neutron scattering on the PRISMA spectromter at the UK ISIS facility. The one-phonon structure factors are calculated to preselect the Bragg points for the measurements and to assign measured phonon signals to different branches. The phonon dispersion relations measured are in good agreement with the calculations.

I. INTRODUCTION

The silicate mineral zircon, $ZrSiO_4$, is found in igneous rocks and sediments and is a host mineral for radioactive elements uranium and thorium in the Earth's crust. It is a natural candidate for usage as a nuclear waste storage material. Zircon is used as a gem stone because of its good optical quality and resistance to the chemical attack. It has a hardness of 7.5 on Mohr scale and a high refractive index. Zircon finds useful industrial applications due to its low thermal conductivity and high melting point. Especially it is a good refractory material as it has a low thermal expansion and good thermal shock resistance. The compressibility[1] and thermal expansion[2] of zircon is lowest among the oxygen based compounds. The specific heat and elastic constants of zircon have also been measured.[3,4]

A phase transition from zircon to scheelite structure has been observed by several workers in static high pressure[5–8] and shock experiments[9] at somewhat different values of pressures and temperatures. It is observed at 12 GPa and 900°C by x-ray-diffraction experiment in a Bridgman-anvil apparatus, at 15 GPa and 1000 °C in a laser-heated diamond cell, and at 23 GPa in a high pressure Raman experiment. A high-temperature neutron powder-diffraction study[10] of zircon carried out up to 1900 K showed a displacive phase transition at 1100 K, and decomposition of $ZrSiO_4$ into β-cristobalite and ZrO_2 at a temperature around 1750 K.

The long-wavelength Raman and infrared active phonons have also been measured at room temperature and pressure.[11] However, these measurements give information only about the zone-center modes. Inelastic neutron scattering is used to obtain information about the phonons in the entire Brillouin zone. Earlier we reported[12] measurements of the phonon dispersion relation of zircon at low energies up to 32 meV. The measurements were carried out using a medium energy resolution triple axis spectrometer at the Dhruva reactor at Trombay. The phonon density of states measurements were also reported for zircon.[13] Recently, measurement of phonon dispersion relations and density of states have been reported for $LuPO_4$,[14] which also has the zirconlike structure.

We now report extensive measurements of the phonon dispersion relation of zircon upto 70 meV using PRISMA time-of-flight spectrometer[15] at the UK ISIS facility from a natural single crystal. Measurement of phonon dispersion curves are important for the refinement of reliable interatomic potentials, which may be used in the calculation of thermodynamic properties at high temperature and pressure. We also report lattice dynamical calculations which are used in planning of the neutron experiment and for assignments of the various inelastic signals to different phonons. In this context, perhaps it is pertinent to note that the use of pulsed neutron sources for phonon dispersion measurements has evolved relatively recently during the last decade as compared to the use of continuous reactor sources. While the pulse sources have been used extensively for the measurement of specific phonons in several materials,[16] there are only a few examples of extensive measurements up to high energies, e.g., Al_2O_3, Cr_2O_3.[17] We may note that the present extensive measurements provide also a rare example of studies on minerals of geophysical interest even using reactor sources.

II. CRYSTAL STRUCTURE AND GROUP THEORETICAL ANALYSIS

The structure of zircon (Fig. 1) has been determined from neutron-diffraction studies using a single crystal[18] and polycrystalline samples.[10] Zircon, $ZrSiO_4$, has a body-centered-

 ©2000 The American Physical Society

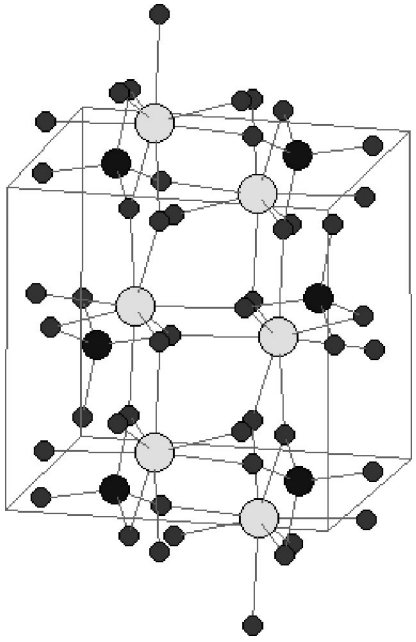

FIG. 1. Crystal structure of zircon $ZrSiO_4$. The solid circles denote Zr, Si, and O atoms in decreasing order of size.

tetragonal structure with space group $I4_1/amd$ and two formula units per primitive cell. The Zr and Si atoms occur at special positions $4a$ and $4b$, respectively, whereas O atoms occur at $16h$. The principle structure unit can be considered as a chain of alternating edge-sharing SiO_4 tetrahedra and ZrO_8 triangular dodecahedra extending parallel to the c axis, with the chain joined along the a axis by edge-sharing ZrO_8 dodecahedra.

The group theoretical analysis of phonon dispersion relation has been carried out using standard techniques.[19] The symmetry decomposition of phonon branches at Γ point, and along the Δ, Λ, and Σ directions are given as

$$\Gamma: \; 2A_{1g}+A_{2g}+A_{1u}+4A_{2u}+4B_{1g}+B_{2g}+B_{1u}+2B_{2u}+5E_g+5E_u,$$

$$\Delta: \quad 8\Delta_1+8\Delta_2+10\Delta_3+10\Delta_4,$$

$$\Lambda: \quad 6\Lambda_1+2\Lambda_2+6\Lambda_3+2\Lambda_4+10\Lambda_5,$$

$$\Sigma: \quad 10\Sigma_1+8\Sigma_2+10\Sigma_3+8\Sigma_4.$$

The results of group theoretical analysis have been used to block diagonalize the dynamical matrices in lattice-dynamical calculations. The group theoretical analysis is useful to distinguish between the various branches and to interpret the experimental result.

III. EXPERIMENT

A natural single crystal with volume 4 cc obtained from the mining site at Puttetti, Tamilnadu, India has been used for the measurements and contains 0.9% of hafnium by weight as the main impurity. The crystal was cooled to 20 K in a helium flow cryostat. In the neutron time-of-flight technique, each detector measures the scattered neutron intensity along a parabolic path in $\mathbf{Q}$-ω space calculated using kinematic equations.[15] For the present experiment, the instrument was configured to use the Prisma-2 single-analyzer detector system, with 11 independently moving analyzer-detector arms. Each arm has a single pyrolitic graphite (002) analyzer and a ^{3}He gas detector. Phonon energies up to 80 meV and corresponding wave vectors can then be extracted from each data set in which the intersections of the 11 detector trajectories with the phonon dispersion relations allows the excitations to be easily mapped out.

We planned the measurement of phonons along [100] and [001] directions. For inelastic neutron scattering from one-phonon excitation, the scattering vector ($\mathbf{Q}$) is given by $\mathbf{Q}=\mathbf{G}\pm\mathbf{q}$, where $\mathbf{G}$ is the Bragg point and $\mathbf{q}$ is phonon wave vector. We calculated the one-phonon structure factors for the neutron inelastic scattering in the a-b and a-c planes for all the Bragg points in the $\mathbf{Q}$ range of $2-8$ Å^{-1}, using a lattice-dynamical model described below. In the a-c plane the structure factors are zero for all the branches in the group theoretical representations Δ_2 and Δ_4 along [100] direction, and in the group theoretical representations Λ_2 and Λ_4 along [001] direction. In the a-b plane, around the Bragg point $(h,k,0)$ $(k=\text{even})$, the structure factors are zero for all the branches in the group theoretical representations Δ_2 and Δ_3 along [100] direction. The above selection rules arise because either the vibrations of the atoms are not in the scattering plane or the phases due to various atoms cancel with each other. The calculation of one phonon structure factors is also used in the assignment of observed inelastic signals to specific phonons branches. Earlier also the calculated phonon intensities were used as guide for the measurements of phonons using single crystals of Mg_2SiO_4 (Ref. 20) and Fe_2SiO_4.[21]

The Bragg points for the measurements are chosen so as to enable measurement of selected phonon branches along a particular direction. We have used (6,0,4), (4,0,4), (5,0,3), and (5,0,4) Bragg points for the measurements in representations Δ_1 and Δ_3 along [100], and (4,0,6), (4,0,4), and (5,0,5) Bragg points for measurements in representations Λ_1, Λ_3, and Λ_5 along [001] directions. Some phonons in representations Δ_1 and Δ_4 along [100] direction are measured using Bragg points (5,4,0) and (6,4,0). Typical time for the measurement of each run is around 20 h to obtain an acceptable signal-to-noise ratio. The structure factors for different branches for scans around the Bragg points (5,4,0) along [100] and (5,0,5) along [001] directions are shown in Figs. 2(a) and 3(a), respectively. The corresponding inelastic scan for one of the detectors in both the directions are also shown in Figs. 2(b) and 3(b), respectively. The inelastic signal is expected for only those branches which have high structure factors.

IV. LATTICE-DYNAMICAL CALCULATIONS

The lattice-dynamics calculations for zircon have been carried out using a shell model.[22,23] The interatomic potential consists of Coulombic and the short-ranged Born-Mayer-type interaction terms

$$V(r)=\frac{e^2}{4\pi\epsilon_0}\frac{Z(k)Z(k')}{r}+a\exp\left(\frac{-br}{R(k)+R(k')}\right)-\frac{C}{r^6}. \tag{1}$$

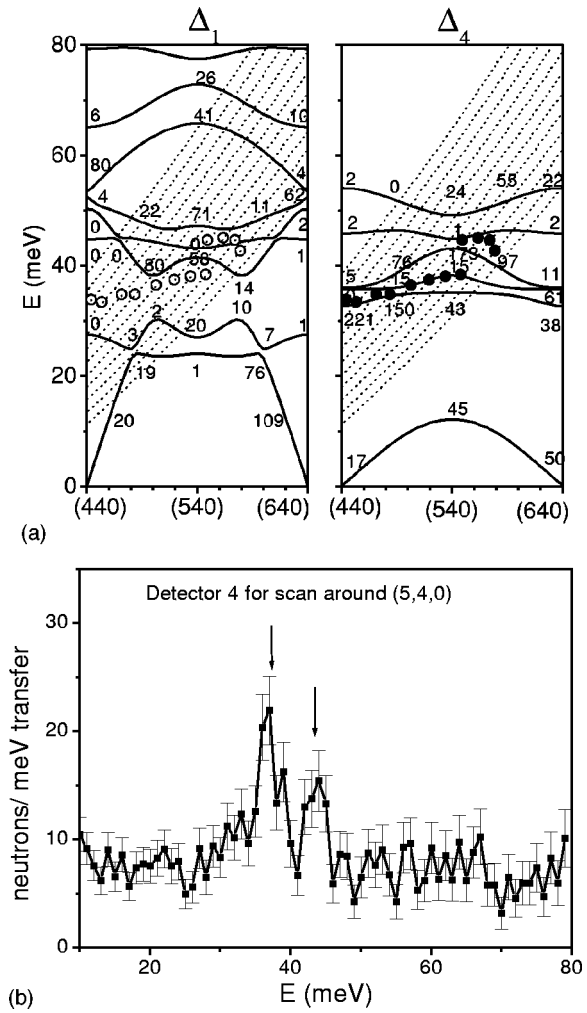

FIG. 2. (a) Information regarding the scan around the Bragg points (5,4,0) along [100] direction. In this scan the structure factor is zero for all the branches in the group theoretical representations Δ_2 and Δ_3 (see text). The full lines give the calculated phonon dispersion relation. The dashed lines give $(\mathbf{Q},\omega)$ path of 11 detectors, respectively. The $(\mathbf{Q},\omega)$ paths of different detectors are plotted from right (number 1) to left (number 11). The numbers on the lines are calculated one phonon structure factors (arbitrary units). The complete experimental data (either filled or open circles) have been plotted in all the possible representations. A preferred assignment to a representation is indicated by filled circles after comparing the intensity of phonons of similar energies in all the representation. However, the same data are plotted in other less preferred representations by open circles. (b) A typical inelastic scan for detector 4. Arrows indicate the peak positions.

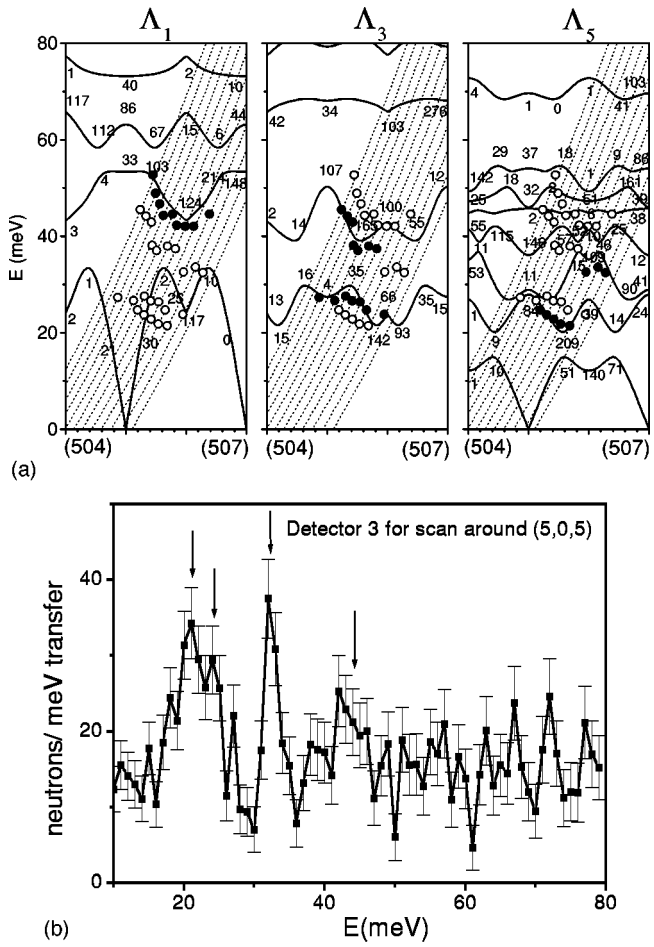

FIG. 3. (a) Information regarding the scan around the Bragg points (5,0,5) along [001] direction. In this scan the structure factor is zero for all the branches in the group theoretical representations Λ_2 and Λ_4 (see text). Description of the lines and the symbols is the same as in Fig. 2(a). (b) A typical inelastic scan for detector 3. Arrows indicate the peak positions.

The van der Waals interaction (last term) in Eq. (1) is applied only between the oxygen atoms. We have also included a Si-O bond stretching potential of the form[22,23]

$$V(r) = -D \exp[-n(r-r_o)^2/(2r)]. \qquad (2)$$

r is the separation between the atoms of a type k and k'. $R(k)$ and $Z(k)$ are the effective radius and charge of the kth atom type. $a = 1822$ eV, $b = 12.364$, and $C = 100$ eV Å^6 are treated as constants; this choice has been successfully used earlier in the lattice-dynamical calculations of several complex solids.[20,21] The parameters used in our calculations are $Z(\mathrm{Zr}) = 3.6$, $Z(\mathrm{Si}) = 2.36$, $Z(\mathrm{O}) = -1.49$, $R(\mathrm{Zr}) = 1.97$ Å, $R(\mathrm{Si}) = 0.88$ Å, $R(\mathrm{O}) = 1.95$ Å, $D = 2.0$ eV, $n = 26.0$ Å^{-1}, $r_o = 1.627$ Å. The polarizibility of the oxygen atoms is introduced in the framework of the shell model[22–24] with the shell charge $Y(\mathrm{O}) = -2.0$ and shell-core force constant $K(\mathrm{O}) = 70$ eV/Å^2. The empirical parameters are optimized to produce the minimum enthalpy structure close to that determined by the diffraction experiments at zero pressure. This minimum enthalpy structure is then used for lattice-dynamical calculations. Further the potential parameters are chosen such that they satisfy the condition of dynamic equilibrium, and long-wavelength phonon modes and elastic constants are close to their experimental values. The potential reproduces the structure of zircon (Table I) quite satisfactory. The calculations have been carried out using the current version of DISPR,[25] developed at Trombay.

V. RESULTS

The observed inelastic signal for some of the detectors are shown in Figs. 2(b) and 3(b) with the peak positions corresponding to the intersection of the detector trajectory with different phonon branches. The $\mathbf{Q}$-ω paths for different detectors for scans around the Bragg points (5,4,0) along [100]

TABLE I. Comparison between the experimental (Ref. 18) (at 293 K) and calculated structural parameters (at 0 K) of zircon. For the space group $I4_1/amd$, the Zr, Si, and O atoms are located at (0,0.75,0.125), (0.0,0.25,0.375), and $(0,u,v)$, respectively, and their symmetry equivalent positions.

	Experimental	Calculated
a (Å)	6.610	6.621
c (Å)	6.001	6.185
u	0.0646	0.069
v	0.1967	0.203

and (5,0,5) along [001] are also shown in Figs. 2(a) and 3(a), respectively. The structure factors for different branches for both the scans are also noted in the same figure. The different representations [Figs. 2(a) and 3(a)] are plotted side a side for comparing the calculated phonon intensities for phonons of similar energies in different representations. The inelastic signal is expected only when the **Q**-ω path for any detector intersects a particular phonon branch which also has a high one-phonon structure factor. The complete experimental data (either filled or open circles) in two typical scans have been plotted in all the possible representations in Figs. 2(a) and 3(a). A preferred assignment to a representation is indicated by filled circles after comparing the intensity of phonons of similar energies in all the representation. However, the same data are plotted in other less preferred representations by open circles. We are able to measure several phonons up to 70 meV. Comparison of all the experimental results (preferred assignments) with the calculations is shown in Fig. 4. The low-energy data[12] measured using the triple axis spectrometer at Dhruva reactor, Trombay are also shown in the same figure. There is a good agreement between the experimental data measured using PRISMA with the low-energy data measured using the triple axis spectrometer[12] and lattice-dynamical calculations. We find that observed phonon intensities are in a good qualitative agreement with the calculated one-phonon structure factors which is quite satisfactory. Some ambiguities in the assignments of the observed experimental data remains as also is the case of similar measurements at a reactor source. The experimental long-wavelength spectroscopic data are also shown in Fig. 4.

The calculated phonon dispersion relation along the three high symmetry directions are shown in Fig. 4. The modes that belong to different group theoretical representations are plotted separately. There is a large gap in the 80–105-meV region. Comparison of the phonon dispersion relation in zir-

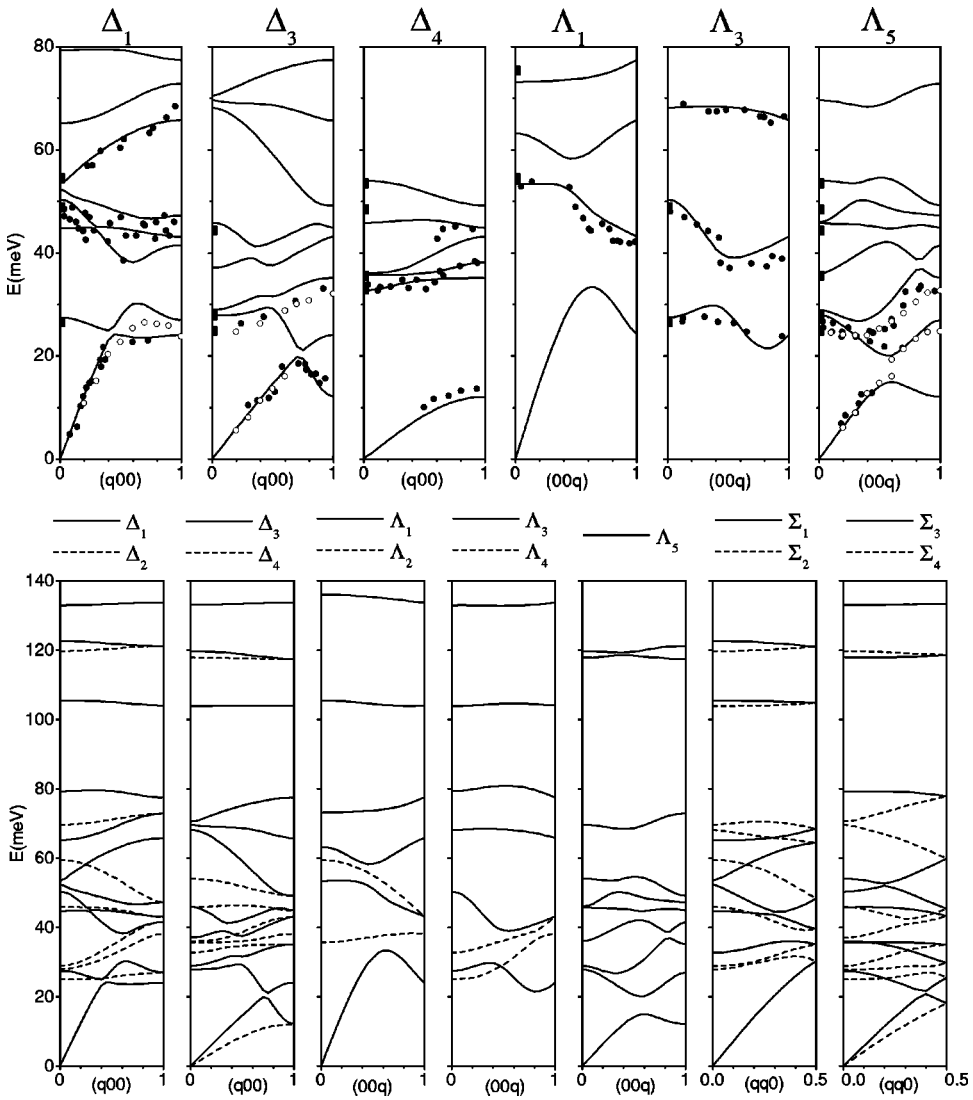

FIG. 4. The experimental phonon data (symbols) along with the lattice-dynamical calculations (lines). The filled and open circles give the phonon peaks identified in the experiments using PRISMA and triple axis spectrometer at Dhruva reactor, Trombay (Ref. 12), respectively. Filled rectangles are the long-wavelength spectroscopic data (Ref. 11). The calculations up to 80 meV for certain representations are plotted in the upper figure for comparsion with the experiments. The lower figure gives the complete phonon dispersion relations.

TABLE II. Comparison between the experimental (Ref. 4) and calculated elastic constants of zircon.

Elastic constant	Experimental (in 10^{11} dynes/cm^2)	Calculated
C_{11}	42.44	45.2
C_{33}	48.96	58.0
C_{44}	11.33	10.2
C_{66}	4.82	3.8
C_{12}	6.92	6.7
C_{13}	15.02	14.8

TABLE III. Comparison of the experimental (Ref. 11) and calculated Raman and infrared modes of zircon.

Representation	Experimental	Calculated (in cm^{-1})
A_{1g}	439	431
	974	850
B_{1g}	214	221
	393	405
		639
	1008	1072
B_{2g}	266	264
E_g	201	225
	225	233
	357	370
		561
	1008	965
A_{2u}(LO)		509
	608	590
	989	1096
A_{2u}(TO)		299
		568
		1073
E_u(LO)		361
		423
		525
		988
E_u(TO)	287	291
	390	369
	431	435
	885	950

con with $LuPO_4$ (Ref. 14) shows that the optic phonons have a larger dispersion in case of zircon.

The calculated elastic constants are in a very good agreement with the experimental data as shown in Table II. In Table III we have compared our calculated long-wavelength Raman and infrared modes with the experimental data. The average deviation of the calculations with optical data is about 5%. The highest frequency modes which involve the stretching vibrations (>800 cm^{-1}) are not as well described (deviations of 4–13%) as the lower frequency modes (deviation from experiments of 1–4% except in one mode showing a deviation of 12%). There is a large LO-TO splitting (Table III) for the A_{2u} and E_u modes. Overall, there is a very good agreement between the calculations and the measured optical frequencies.

VI. CONCLUSIONS

In this paper we have reported detailed lattice-dynamical studies of the mineral zircon using the technique of neutron inelastic scattering and a lattice-dynamical shell model. The model is used for the calculations of one-phonon coherent-inelastic neutron scattering cross sections and thereby planning the inelastic neutron-scattering measurements using a single crystal. The neutron measurements have been carried out using the PRISMA time-of-flight spectrometer at the UK ISIS facility. The present extensive phonon measurements of several phonon branches extending up to 70 meV provides one of the few examples of such studies using a pulse neutron sources on any material. Such extensive measurements have been performed on only a few mineral systems even using a continuous reactor source. The experimental results are in good agreement with our model calculations, which provides the essential support for the interatomic potential as used in this important mineral.

[1] D.B. Sirdeshmukh and K.G. Subhadra, J. Appl. Phys. **46**, 3681 (1975); R.M. Hagen and L.W. Finger, Am. Mineral. **64**, 196 (1979).

[2] A.J. Falzone and F.D. Stacey, Phys. Chem. Miner. **8**, 212 (1982); T.G. Worlton, L. Cartz, A. Niravath, and H. Ozkan, High Temp.-High Press. **4**, 463 (1972); E.C. Subbarao, D.K. Agarwal, H.A. Mckinstry, C.W. Sallese, and R. Roy, J. Am. Ceram. Soc. **73**, 1246 (1989); J.B. Austin, *ibid.* **14**, 795 (1931); E.C. Subbaro and K.U.G.K. Gokhale, Jpn. J. Appl. Phys. **7**, 1126 (1968).

[3] K.K. Kelly, J. Am. Chem. Soc. **63**, 2750 (1941).

[4] H. Ozkan and J.C. Jamieson, Phys. Chem. Miner. **2**, 215 (1978).

[5] A.F. Reid and A.E. Ringwood, Earth Planet. Sci. Lett. **6**, 205 (1969).

[6] A.E. Ringwood, *Composition and Petrology of the Earth's Mantle* (McGraw-Hill, New York, 1975).

[7] L.G. Liu, Earth Planet. Sci. Lett. **44**, 390 (1979).

[8] E. Knittle, Q. Williams, Am. Mineral. **78**, 245 (1993).

[9] K. Kusuba, Y. Syono, M. Kikuchi, and K. Fukuoka, Earth Planet. Sci. Lett. **72**, 433 (1985).

[10] Z. Mursic, T. Vogt, and F. Fray, Acta Crystallogr., Sect. B: Struct. Sci. **B48**, 584 (1992).

[11] P. Dawson, M.M. Hargreave, and G.R. Wilkinson, J. Phys. C **4**, 240 (1971).

[12] R. Mittal, S.L. Chaplot, Mala N. Rao, N. Choudhury, and R. Parthasarthy, Physica B **241**, 403 (1998).
[13] J.C. Nipko and C.-K. Loong, Physica B **241**, 415 (1998).
[14] J.C. Nipko, C.-K. Loong, M. Lowenhaupt, M. Braden, W. Reichardt, and L.A. Boatner, Phys. Rev. B **56**, 11 584 (1997).
[15] U. Steigenberger, M. Hagen, R. Caciuffo, C. Petrillo, F. Cilloco, and F. Sacchelti, Nucl. Instrum. Methods Phys. Res. B **53**, 87 (1991).
[16] M.J. Harris, M.E. Hagen, M.T. Dove, and I.P. Swainson, J. Phys.: Condens. Matter **10**, 6851 (1998); M.J. Harris, M.T. Dove, and K.W. Godfrey, Phys. Rev. B **51**, 6758 (1995).
[17] G. Artioli, A. Pavese, and O. Moze, Am. Mineral. **81**, 19 (1996); B. Dorner, J. Neutron Res. **2**, 115 (1994); H. Schober, T. May, B. Dorner, D. Strauch, U. Steigenberger, and Y. Morrii, Z. Phys. B: Condens. Matter **98**, 197 (1995).
[18] Z. Mursic, T. Vogt, H. Boysen, and F. Frey, J. Appl. Crystallogr. **25**, 519 (1992).
[19] O.V. Kovalev, *Irreducible Representations of Space Groups* (Gordon and Breach, New York, 1964); C.J. Bradely and A.P. Cracknell, *The Mathematical Theory of Symmetry in Solids* (Oxford University Press, Oxford, 1972).
[20] S. Ghose, J.M. Hastings, L.M. Corliss, K.R. Rao, S.L. Chaplot, and N. Choudhury, Solid State Commun. **63**, 1045 (1987); K.R. Rao, S.L. Chaplot, N. Choudhury, S. Ghose, J.M. Hastings, L.M. Corliss, and D.L. Price, Phys. Chem. Miner. **16**, 83 (1988).
[21] S. Ghose, J.M. Hastings, N. Choudhury, S.L. Chaplot, and K.R. Rao, Physica B **174**, 83 (1991).
[22] R. Mittal and S.L. Chaplot, Phys. Rev. B **60**, 7234 (1999).
[23] R. Mittal, S.L. Chaplot, N. Choudhury, and C.-K. Loong, Phys. Rev. B **61**, 3983 (2000).
[24] P. Bruesch, *Phonons: Theory and Experiments* (Springer, Berlin, 1982), Vol. 1.
[25] S.L. Chaplot (unpublished).